Kinetics and Rate Constants of the Reaction $CH_2OH + O_2 \rightarrow CH_2O + HO_2$ in the Temperature Range of 236−600 K†

Alexander Schocker,[‡,§,⊥] Masanori Uetake,[||] Nozomu Kanno,[§] Mitsuo Koshi,[||] and Kenichi Tonokura*[*,§,||]

Physikalische Chemie I, Universität Bielefeld, Universitätsstrasse 25, D-33615 Bielefeld, Germany, Department of Chemical System Engineering, School of Engineering, The University of Tokyo, 7-3-1 Hongo, Bunkyo-ku, Tokyo 113-8656, Japan, and Environmental Science Center, The University of Tokyo, 7-3-1 Hongo, Bunkyo-ku, Tokyo 113-0033, Japan

Received: December 1, 2006; In Final Form: January 28, 2007

The kinetics and absolute rate constants of the gas-phase reaction of the hydroxymethyl radical (CH_2OH) with molecular oxygen have been studied using laser photolysis/near-IR absorption spectroscopy. The reaction was tracked by monitoring the time-dependent changes in the production of the hydroperoxy radical (HO_2) concentration. For sensitive detection of HO_2, two-tone frequency modulation absorption spectroscopy was used in combination with a Herriott-type optical multipass absorption cell. Rate constants were determined as a function of temperature (236 K < T < 600 K) at 50 Torr of N_2. The experimental results exhibit a slight negative temperature dependence in the measured temperature region. Microcanonical variational transition state theory was used to estimate the rate constants of the investigated reaction. The results of the theoretical calculations also suggest a negative temperature dependence of the reaction rate constant in the measured temperature region.

1. Introduction

Modeling and especially the development of suitable reaction mechanisms are essential for a better understanding of complex chemical processes, for example, combustion, catalysis, or atmospheric chemistry. Experimental studies provide the fundamental data for such models and reaction mechanisms. Consequently, the comparison between experimental and theoretical data allows the improvement of models and is a crucial test for the validation of reaction mechanisms.[1−4]

Reactions of α-hydroxyalkyl radicals (RCHOH) with molecular oxygen are important elementary reactions in environmental and atmospheric chemistry. In particular, the oxidation reaction of the simplest α-hydroxyalkyl radical—the hydroxymethyl radical (CH_2OH)—plays a significant role in the last stage of the isoprene degradation processes in the troposphere.[1,5] In experimental studies, the hydroxymethyl radical is often used as a model compound for reactions between α-hydroxyalkyl radicals and reactive molecules such as oxygen or nitrogen oxides.

In the atmosphere, CH_2OH reacts mainly with molecular oxygen, which results in the formation of formaldehyde (CH_2O) and the hydroperoxy radical (HO_2):[6−8]

$$CH_2OH + O_2 \rightarrow CH_2O + HO_2 \qquad (1)$$

In addition, this reaction is of interest to researchers in combustion chemistry, because CH_2OH is a key radical in methanol flames.[9−13] Much effort has been made to investigate the kinetics of this reaction.[9,14−25] Table 1 summarizes recent studies, the majority of which report rate constants around room temperature.[9,14,18−25] The only exceptions to this are the studies of Grotheer et al.[9] and Nesbitt et al.[22] who reported rate constants at above and below room temperature, respectively. Both studies represent typical temperatures in atmospheric and low-temperature combustion chemistry.

The rate constant values of Grotheer et al.[9] showed the reaction to have a complex, non-Arrhenius behavior in the temperature dependence of these data with a minimum rate constant at around 500 K. These observations could be explained by a change in mechanism with temperature, such as addition−/rearrangement−/decomposition pathways as well as addition and elimination pathways. In contrast, Nesbitt et al. observed a positive temperature dependence of the rate constants below 300 K.[22] However, significant uncertainties of the reaction mechanism still remain.

Recent theoretical quantum chemical calculations have indicated a revision of the reaction mechanisms.[8,26−28] Olivella et al.[26] calculated a potential energy surface (PES) of the $CH_2OH + O_2$ reaction system at the CCSD(T)/cc-pVTZ//CASSCF/6-311G(d,p) level of theory. From the calculated PES, they indicated that the addition and elimination pathway would be dominant around room temperature. Dibble[8] performed RRKM (Rice−Ramsperger−Kassel−Marcus)-Master Equation calculations to estimate the fraction of the chemically activated $HOCH_2OO$ radical quenched at various pressures and temperatures. In the RRKM-Master Equation calculations, the microcanonical rate constants of the entrance channel ($CH_2OH + O_2 \rightarrow HOCH_2OO$) were estimated from the inverse Laplace transformation, assuming the value of the Arrhenius pre-

† Part of the special issue "M. C. Lin Festschrift".

* Corresponding author. Fax: +81-3-5841-2119. E-mail: tonokura@esc.u-tokyo.ac.jp.

‡ Universität Bielefeld.

§ Environmental Science Center, The University of Tokyo.

|| Department of Chemical System Engineering, School of Engineering, The University of Tokyo.

⊥ Present address: BASF AG, Competence Center for Process Analytical Technology, WLE/EB − L426, Carl-Bosch-Strasse 38, D-67056 Ludwigshafen, Germany.

10.1021/jp0682513 CCC: $37.00
Published on Web 03/14/2007

TABLE 1: Overview of the Measured Rate Constants for the Reaction $CH_2OH + O_2 \rightarrow CH_2O + HO_2$[i]

rate constant 10^{-12} cm^3 molecule^{-1} s^{-1}	pressure (Torr)	temperature (K)	technique[a]	ref
9.2 (298 K)	0.98−1.93	298−682[b]	DF-MS[c]	9
2^{+2}_{-1}	0.5	300	DF-LMR[d]	14
16.6	900−19000	1200−1800	methanol oxidation in shock tube	15
	40	1000−2000[e]	lean methanol flame	16
	40	1000−2000[f]	lean methanol flame	17
1.4 ± 0.4	1−3	RT[g]	DF-PFE[d]	18
9.5 ± 2.5	0.3−0.9	RT[g]	DF-MS[c]	19
10.6 ± 2.5	0.52−4.88	298	DF-LMR[c,d]	20
8.6 ± 2.0	1	298	DF-MS[c]	21
8.61 ± 1.14 (300 K)	1	215−300[h]	DF-MS[c]	22
8.8 ± 0.2	760	298	PR-AS (UV)[c]	23
11.7 ± 1.2	1.3−5.5	296 ± 4	PLP-PIMS[c]	24
10 ± 1.4	5.8−15.2	294 ± 2	PLP-TDLA[d]	25

[a] DF: discharge flow; PFE: photofragment emission; LMR: laser magnetic resonance; MS: mass spectrometry; PR: pulse radiolysis; AS: absorption spectroscopy; PLP: pulsed laser photolysis; PIMS: photoionization mass spectrometry; TDLA: tunable diode laser absorption. [b] $2.5 \times 10^{-9}\ T^{-1} + 4.0 \times 10^{-9} \exp(-2525/T)$. [c] Monitoring CH_2OH. [d] Monitoring HO_2. [e] $1.7 \times 10^{-10} \exp(-2500/T)$. [f] $1.66 \times 10^{-10} \exp(-3019/T)$. [g] Room temperature. [h] $5.6 \times 10^{-9} \exp(-1700/T)$ at 215−250 K. [i] The table summarizes reported values from previous studies together with experimental conditions and detection techniques.

TABLE 2: Concentrations of the Precursor Molecules

species	concentration molecules cm^{-3}
Cl_2	$(0.5-2) \times 10^{15}$
CH_3OH	4×10^{16}
O_2	$(2-8) \times 10^{15}$

exponential factor for the reverse reaction at high-pressure limit to be 2×10^{15} s^{-1}. Thus, the absolute rate constants were not predicted. Hermans et al.[27] calculated a PES of the formation and decomposition of α-hydroxy-alkylperoxyl radical including $HOCH_2OO$ at G3 and G2M//B3LYP/cc-pVTZ methods. They also estimated the fraction of the chemically activated $HOCH_2OO$ using RRKM-Master Equation calculations. Ramírez-Ramírez et al.[28] calculated a PES of the $CH_2OH + O_2$ reaction system at the QCISD(T)/6-311+G(2df,2p)//QCISD/6-31G(d) level of theory. Although they found a saddle point at the entrance of the reaction, the transition state showed a significant amount of spin contamination.

Despite the considerable effort that was made, significant uncertainties still remain. To improve our understanding of the detailed reaction mechanism, further experimental studies of the rate constants are desirable. It is important to note that different experimental setups were used in the past for the studies described above. The aim of this work is to conduct a comprehensive study of the rate constants over a wide temperature range, while using only one single experimental setup. In this way, optimum comparability of the results over the entire temperature range can be achieved.

2. Experimental Details

The kinetic experiments for the determination of the rate constants were performed using a temperature-regulated photolysis flow cell that is similar to the setup used in previous studies.[29−32] In the following, the setup will be reviewed briefly, and modifications will be described in detail.

2.1. Photolysis Flow Cell. The reaction $CH_2OH + O_2 \rightarrow CH_2O + HO_2$ was initiated inside the flow cell by a photolysis laser beam. A well-defined gas mixture containing $Cl_2/CH_3OH/N_2$ and O_2 was flushed through the cell continuously. The typical concentrations of the reactants are summarized in Table 2. The flow rates of the gas mixture inside the reactor were controlled by calibrated mass flow controllers (Kofloc 3660), while the total pressure (constant at 50 Torr) was measured near the exit of the flow cell with a capacitance manometer (MKS Baratron 622A). The temperature inside the flow cell was regulated in the following ways. For temperatures below room temperature, a cooling jacket with methanol as coolant was used. The gas mixtures passed a pre-cooling module before being introduced into the flow cell. To maintain temperatures higher than room temperature, an electric heater with three independent and adjustable heating zones was used. To ensure that the temperature of the reaction gas mixture inside the cell was preheated to the applicable value, the temperature of the two boundary layers of the thermo heater was adjusted to be 10% higher than in the center. This guarantees that the temperature in the detection zone (see below) was almost constant. The temperature profile inside the flow cell was determined before starting the measurements.

The reaction mixture of the precursor molecules was irradiated by laser pulses (THG: 355 nm; power: 100 mJ cm^{-2}) generated by a Nd:YAG laser (Continuum Surelite II). In this way, the photolysis of Cl_2 was initiated and CH_2OH was formed by the following reactions:

$$Cl_2 + h\nu \rightarrow 2Cl \quad (2)$$

$$Cl + CH_3OH \rightarrow CH_2OH + HCl \quad (3)$$

Since the gas residence time was in the range of 1−2 s, kinetic experiments were performed using a laser repetition of 0.5−1 Hz to ensure removal of the reacted mixture and replenishment of the gas sample between successive laser shots.

2.2. Optical Detection by TTFM Absorption Spectroscopy. The progress of the reaction $CH_2OH + O_2 \rightarrow CH_2O + HO_2$ was monitored by the time-dependent changes of the hydroperoxy radical concentration [HO_2]. Two-tone frequency modulation (TTFM) absorption spectroscopy was used for the sensitive detection of HO_2. In the near-IR region, HO_2 shows structured absorption bands.[33,34] The $9_{1,9} \leftarrow 9_{0,9}$ F_1-line of the HO_2 $\tilde{A}^2A' \leftarrow \tilde{X}^2A''$ 000−000 band at 7039.74 cm^{-1} was chosen for the detection and monitoring below room temperature, while the $18_{1,18} \leftarrow 18_{0,18}$ F_2-line of the same band at 7013.52 cm^{-1} was chosen above 350 K, since the population of the rotational quantum state differs between the high- and low-temperature regions.

The probe laser beam was generated by a cw-tunable diode laser (New Focus Velocity 6327), and the frequency was modulated at two closely separated radio frequencies (600 ±

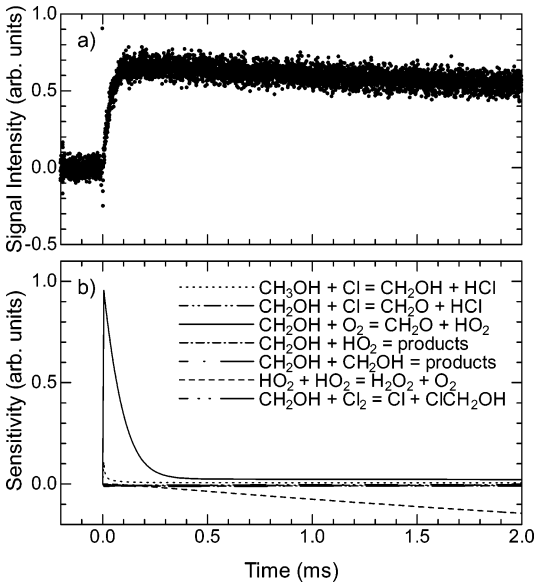

Figure 1. (a) Typical time-dependent concentration profile of HO_2 detected by TTFM spectroscopy at 298 K. The concentrations of Cl_2, O_2, and CH_3OH in the flow cell were adjusted to 1.0×10^{15}, 2.5×10^{15}, and 4.0×10^{16} molecules cm^{-3}, respectively. (b) Sensitivity analysis of the temporal changes in the HO_2 concentration performed with CHEMKIN 4.0 (see text). Details for the seven reactions with high sensitivities for HO_2 concentration can be found in Table 3. The analysis suggests that the rise part is governed mainly by the $CH_2OH + O_2$ reaction, while the decay part is due to the self-reaction of HO_2. Other reactions are almost insensitive and show no significant contribution to the changes in the HO_2 concentration profiles.

2.6 MHz) in a MgO:$LiNbO_3$ crystal, housed in an external resonant cavity (New Focus 4423M). The frequency of the laser output was monitored during the entire measurements using a wave meter (Burleigh WA-1500). To increase the absorption path length and thus the sensitivity according to the Lambert−Beer law, the flow cell was designed in a Herriott-type optical multipassing configuration. In this configuration, the probe beam passes the flow cell 23 times before it reaches the InGaAs photovoltaic detector (New Focus 1811FSM). The overlap of the pump beam and the probe beam was about 64 cm in which the radical concentrations at all points were essentially the same. Assuming a spatial overlap of ≈64 cm between the photolysis and the probe beam (single-pass absorption), the effective absorption path length is extended up to ≈15 m. Finally, the transmitted radiation was heterodyne-detected at twice the intermodulation frequency (2×2.6 MHz = 5.2 MHz) and amplified with a low-noise preamplifier (Stanford Research Systems SR 560). Differential attenuation of either the carrier or the side bands unbalances the phase-modulated light and generates a beat note in the detector photocurrent whose amplitude is proportional to the absorption.[35] The time-dependent concentration profile of HO_2 was derived from this signal. After averaging with a digital oscilloscope (Tektronix TDS 520A) over 500−1000 laser shots, the curve was transferred to a personal computer via GPIB. For a given temperature, up to nine temporal concentration profiles at different O_2 concentrations were recorded.

3. Results and Discussion

3.1. Data Evaluation and Sensitivity Analysis. A typical concentration profile of HO_2 produced from the reaction of CH_2OH with O_2 is shown in Figure 1a. The concentration profile of HO_2 might be affected by reactions such as the HO_2 self-reaction and the $HO_2 + CH_2OH$ reaction. Moreover, the reaction of CH_2OH with Cl and Cl_2 might compete with the investigated reaction shown in eq 1. Therefore, it is necessary to consider potential side reactions before starting the evaluation. Thus, we first carried out a computer-based sensitivity analysis. This analysis of the time-dependent changes in the HO_2 concentration was performed by the CHEMKIN 4.0 program suite[36] and includes 37 reactions. Seven of these reactions with a high sensitivity for the HO_2 concentration[19,24,37−41] are listed in Table 3. As shown in Figure 1b, the results of the sensitivity analysis suggest that the rise part is mainly governed by the reaction shown in eq 1, while the decay part is due to the self-reaction of HO_2 resulting in the formation of H_2O_2 and O_2. The self-reaction follows a second-order kinetic law and has to be considered in the evaluation:

TABLE 3: The Sensitivity Analysis of the $CH_2OH + O_2$ Reaction Kinetics Contains 37 Reactions, of Which This Table Presents Seven Reactions with a High Sensitivity

reaction	rate constant @ 298 K cm^3 $molecule^{-1}$ s^{-1}	ref
$CH_2OH + HO_2 \rightarrow$ products	6.0×10^{-11}	19
$CH_2OH + O_2 \rightarrow CH_2O + HO_2$	1.2×10^{-11}	24
$Cl + CH_3OH \rightarrow CH_2OH + HCl$	5.3×10^{-11}	37
$CH_2OH + Cl \rightarrow CH_2O + HCl$	6.6×10^{-10}	38
$CH_2OH + CH_2OH \rightarrow$ products	1.5×10^{-11}	39
$HO_2 + HO_2 \rightarrow H_2O_2 + O_2$	1.9×10^{-12}	40
$CH_2OH + Cl_2 \rightarrow ClCH_2OH + Cl$	2.7×10^{-11}	41

$$HO_2 + HO_2 \rightarrow H_2O_2 + O_2 \qquad (4)$$

Other reactions are almost insensitive, that is, they have a negligible contribution to the time-dependent concentration profile of HO_2. In general, the reaction shown in eq 1 under investigation is well represented by second-order kinetics, and could thus be regarded as pseudo first-order kinetics under a surplus of O_2. For the evaluation of the raw data, a Levenberg−Marquardt (weighted least-squares) fit was applied using the following equation:

$$\frac{d[HO_2]}{dt} = [CH_2OH]_0 \times \{1 - \exp(-k't)\} - 2k_4[HO_2]^2 \qquad (5)$$

where $[CH_2OH]_0$ is the initial concentration of hydroxymethyl radical, k' is the pseudo first-order rate constant of the reaction of the hydroxymethyl radical with O_2, and k_4 is the second-order rate constant of the self-reaction of HO_2 (eq 4). Since the absorption cross sections of HO_2 in the near-IR spectral region are not known, the absolute concentration of the hydroperoxy radical $[HO_2]$ and the initial concentration of the hydroxymethyl radical $[CH_2OH]_0$ cannot be derived directly from the signal intensity. Therefore, an assumption is necessary to obtain these values. In a large excess of O_2, reaction 1 proceeds rapidly, thus the time profile of $[HO_2]$ is controlled only by reaction 4. Under such conditions, we can determine $k_4[HO_2]_0$ from the second-order kinetic analysis, where $[HO_2]_0$ can be regarded to be equal to $[CH_2OH]_0$ in the main experiments. Considering published data, we assumed the rate constant of the HO_2 self-reaction (eq 4) to be $k_4 = 1.87 \times 10^{-12}$ cm^3 $molecule^{-1}$ s^{-1} with N_2 as the diluent at 297 K and 50 Torr.[40,42,43] Because the Cl quantum yield in the 355-nm photolysis of Cl_2 are almost constant as a function of temperature, the initial concentration of the hydroxymethyl radical for higher and lower temperatures can readily be estimated from this value. The determined concentrations of the initial hydroxymethyl radical were in the range of $(1.6-5.4) \times 10^{13}$ molecules cm^{-3}. Although a higher methanol concentration was required to minimize the influence

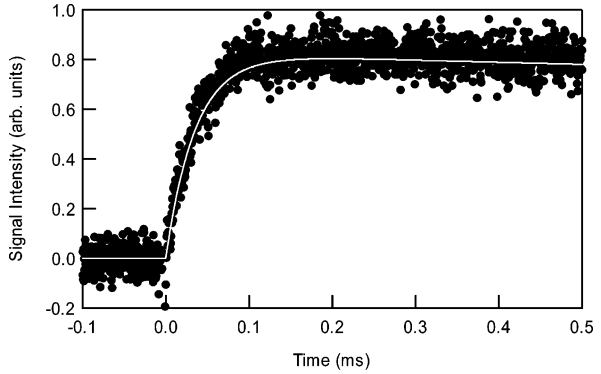

Figure 2. Typical temporal concentration profile of HO_2 measured at 297 K. The concentrations of Cl_2, O_2, and CH_3OH in the flow cell were adjusted to 1.0×10^{15}, 2.5×10^{15}, and 4.0×10^{16} molecules cm^{-3}, respectively.

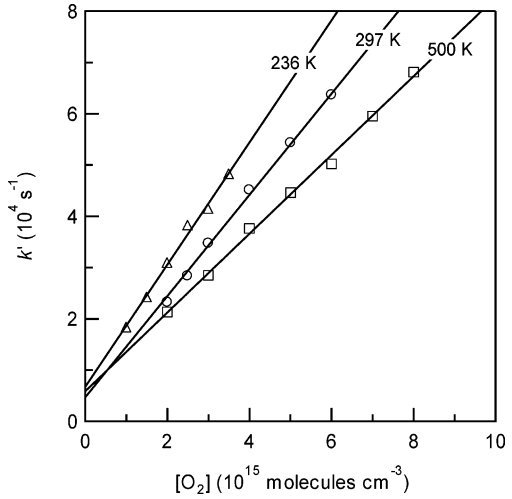

Figure 3. Plots of the pseudo first-order rate constant k' versus O_2 concentration for $T = 236$, 297, and 500 K. All measurements show a perfect linear correlation.

of side reactions in the main experiments, the self-reaction of HO_2 is enhanced by methanol.[40,43,44] Thus, the value of k_4 used in the analysis of eq 5 was measured under the same methanol concentrations and at large excess of O_2 before measuring the rate constants of the $CH_2OH + O_2$ reaction.

3.2. Rate Constants. Figure 2 shows a typical concentration profile including the fitted curve. In all experiments, the concentration profiles were well represented by eq 5, which implies the contribution of the side reactions other than reaction 4 were negligible. From the nonlinear least-squares fitting of eq 5, the pseudo first-order rate coefficient k' was deduced. Plotting these values against the oxygen concentration $[O_2]$, the final rate constants k_1 for the reaction of CH_2OH with O_2 are determined by a linear least-squares analysis. Some typical examples for $T = 236$, 297, and 500 K are shown in Figure 3 and indicate an excellent linear correlation. For room temperature (297 K) a rate constant of $k_1 = (9.9 \pm 0.5) \times 10^{-12}$ cm^3 $molecule^{-1}$ s^{-1} is determined, where error indicates 2σ of the linear least-square analysis. This result is in excellent agreement with numerous previous studies at room temperature[9,19−25] and confirms the calibration of the experimental setup. A series of experiments was carried out at various temperatures. The complete results are summarized in Table 4 and are presented in Figure 4. The maximum rate constant of $(11.9 \pm 1.0) \times 10^{-12}$ cm^3 $molecule^{-1}$ s^{-1} is measured at 236 K, while the minimum is found to be $(5.8 \pm 1.3) \times 10^{-12}$ cm^3 $molecule^{-1}$ s^{-1} at 600 K.

To our knowledge, these are the first measurements that cover a large temperature range while using only one single experimental setup. We confirmed no pressure dependence of the rate constant in the pressure range up to 50 Torr, which is consistent with previous studies.[9,19−25]

3.3. Comparison to Previous Studies. For a detailed comparison, our results are presented in Figure 4 together with the data of previous studies. A reasonable agreement can be found between our data and the rate constants in the mid-temperature range (297−500 K) reported by Grotheer et al.[9] In contrast, deviations are obvious for temperatures higher than 500 K. While Grotheer et al. observed a strong increase in the rate constant for temperatures above 500 K, we found a further decrease in the temperature dependence. These deviations were most significant at 600 K, which is the highest temperature in this study.

Nesbitt et al. measured the reaction rate coefficients for the temperature range from 300 to 215 K using discharged flow technique and found a strong decrease from 8.61×10^{-12} to 2.46×10^{-12} cm^3 $molecule^{-1}$ s^{-1}.[22] They explained this complex temperature dependence by suggesting an isomerization of the transition state from the $OOCH_2OH$ radical (at low temperatures) to the OCH_2OOH radical. In contrast, our results show a slight increase of the rate constants in this range, up to 11.9×10^{-12} cm^3 $molecule^{-1}$ s^{-1} and suggest that the temperature range of 236−600 K exhibits a negative temperature dependence. The reason for the differences between our results and those of Nesbitt et al. is not clear. The negative temperature dependence of the rate constants observed in the present work is characteristic of an association/decomposition channel and very similar to that of the $HCO + O_2$ reaction.[45,46] According to the PES reported by Olivella et al.,[26] the first step of the $CH_2OH + O_2$ reaction is the formation of the $OOCH_2OH$ peroxy radical without surmounting an energy barrier. The negative temperature dependence would be caused by this association reaction. Dibble performed RRKM-Master Equation calculations to follow the time-dependent changes of the intermediates of the $CH_2OH + O_2$ reaction.[8] The chemically activated $OOCH_2OH$ is transferred to $CH_2OH + HO_2$ within 50 ps at 298 K in 760 Torr of N_2. The fraction of chemically activated $OOCH_2OH$ radicals dissociating to $CH_2OH + O_2$ increased with an increasing temperature. This result underlines the negative temperature dependence of an entrance association/decomposition channel.

3.4. Comparison with Theoretical Calculations. We performed quantum chemical calculations of the PES of the $CH_2OH + O_2$ reaction system. Figure 5 shows the PES of the doublet ground state calculated at the G3//B3LYP/6-31G(d)[47] level of theory using Gaussian 03 program suites.[48] The optimized structures of reactants, intermediates, products and transition states are found in the Supporting Information for this paper. We found four local minima, $OOCH_2OH$, OCH_2OOH, and two kinds of CH_2O-HO_2 complexes. In one of the CH_2O-HO_2 complexes, CH_2O and HO_2 were located in the same plane, as Olivella et al. reported.[26] In the other complex, HO_2 was located perpendicular to CH_2O. The stabilization energies of these complexes from the reactants were calculated to be −26.7 and −24.7 kcal mol^{-1}, respectively. The intrinsic reaction coordinate scan from the transition state between $OOCH_2OH$ and CH_2O-HO_2 revealed that the perpendicular CH_2O-HO_2 complex was related to the $CH_2OH + O_2$ reaction system. This agrees with Anglada and Domingo.[49] The stabilization energies of $OOCH_2OH$ and OCH_2OOH from the reactants were −34.7 and −17.0 kcal mol^{-1}. These results are in good agreement with reported values.[26−28] As Olivella et al. stated,[26] the transition state

TABLE 4: Measured Rate Constant Results for the Reaction $CH_2OH + O_2 \rightarrow CH_2O + HO_2$ in the Temperature Range 236−600 K[a,b]

temperature (K)	$[CH_3OH]$ 10^{16} molecules cm^{-3}	$[Cl_2]$ 10^{15} molecules cm^{-3}	$[O_2]$ 10^{15} molecules cm^{-3}	rate constant 10^{-12} cm^3 $molecule^{-1}$ s^{-1}
236	4.0	0.5−1.0	1.0−3.5	11.9 ± 1.0
250	4.0	0.5−1.0	1.0−4.0	10.2 ± 0.8
273	4.0	0.5−1.0	1.0−4.0	9.1 ± 0.7
297	4.0	3.0	1.5−7.0	10.0 ± 0.4
297	4.0−8.0	1.0	1.5−7.0	9.9 ± 0.5
350	4.0−8.0	1.5−2.0	2.0−8.0	8.4 ± 0.7
400	4.0−8.0	1.5−2.0	2.0−8.0	7.8 ± 0.6
500	4.0−8.0	1.5−2.0	2.0−8.0	7.7 ± 0.4
550	4.0	1.5	2.0−7.0	8.2 ± 0.9
600	4.0−8.0	1.5	2.0−6.0	5.7 ± 1.3
600	4.0	1.5	2.0−7.0	6.5 ± 0.4

[a] This table includes experimental conditions of the precursor molecules. [b] The total pressure was kept constant at 50 Torr.

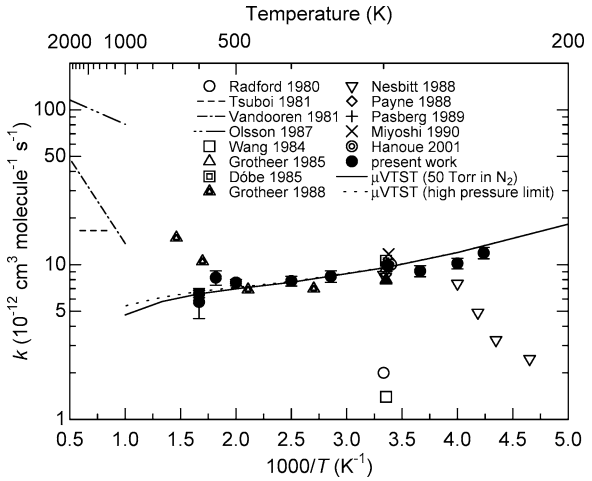

Figure 4. Arrhenius plot for the reaction $CH_2OH + O_2 \rightarrow CH_2O + HO_2$. The figure includes the determined rate constants measured in previous studies (see Table 4 for the exact values). For the sake of completeness, the former data from Radford[14] and Wang et al.[18] measured at room temperature are also included.

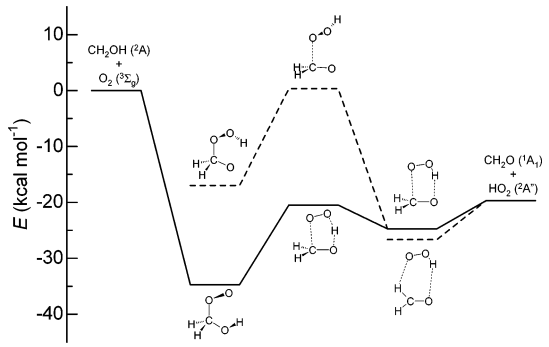

Figure 5. Schematic potential energy profiles showing the most relevant structures and transition states for the reaction $CH_2OH + O_2 \rightarrow CH_2O + HO_2$. This figure is based on quantum chemical calculations at the G3//B3LYP/6-31G(d) level of theory. The reaction channels indicated in dashed lines are omitted in the calculations of the rate constants (see text).

between $OOCH_2OH$ and OCH_2OOH and the four-member ringed transition state between the $OOCH_2OH$ and CH_2O-HO_2 complex were not found at the B3LYP/6-31G(d) level of theory.

In contrast to Ramírez-Ramírez et al.,[28] the saddle point ("tight" transition state) of the entrance channel was not found in our calculations. They reported that the optimization of the saddle point was sensitive to the calculation level. Moreover, the spin-contamination at optimized structure was quite large. To estimate the reaction rate constant of the entrance channel, the energies and harmonic frequencies of CH_2OH-O_2 are required as a function of intermolecular distance. We performed the PES scan of the C−O length of $OOCH_2OH$ up to 4.7 Å at the B3LYP/6-31G(d) level and scaled the PES by the ratio of stabilization energy of $OOCH_2OH$ at the G3//B3LYP/6-31G(d) level and at the B3LYP/6-31G(d) level. We fixed the O−H bond length in the scanning procedure to avoid the PES scan toward to the transition state between $OOCH_2OH$ and CH_2O-HO_2. The induced error of the CH_2OH energy due to the frozen O−H distance is 0.06 kcal mol^{-1} at the G3//B3LYP/6-31G(d) level of theory, which is 0.2% of the stabilization energy of $OOCH_2OH$. At the larger intermolecular distances, the spin contamination becomes large. This situation often occurs in the doublet + triplet bimolecular systems.

The calculations of the rate constants of the $CH_2OH + O_2$ reaction were performed by Variflex code.[50] For the calculations, OCH_2OOH and the related transition states were omitted due to the high-energy barrier. The density of states of each species and the sum of states of the transition states were calculated in the rigid rotor-harmonic oscillator approximation. The transition state of the entrance channel was determined variationally in a microcanonical way, that is, determined variationally at each energy, E, and the total angular momentum quantum number, J. In all master equation calculations we used the single-exponential down model for the energy transfer function with $\Delta E_{down} = 200$ cm^{-1}.

The values of the calculated rate constant at 50 Torr in N_2 and the high-pressure limit are included in Figure 4 as solid and dotted lines. Below room temperature, the rate constants calculated by the microcanonical variational transition state theory (μVTST) are insensitive to the total pressure. At 298 K, the calculated rate constants at 50 Torr in N_2 and the low- and high-pressure limits are 9.58×10^{-12}, 9.58×10^{-12}, and 9.61×10^{-12} cm^3 $molecule^{-1}$ s^{-1}, respectively. At higher temperatures, a slight pressure dependence of the rate constants appears, while the rate constants are almost independent of pressures below 50 Torr. In our calculations, the reaction of $CH_2OH + O_2$ finally produces CH_2O and HO_2, which is in good agreement with the theoretical studies of Dibble[8] and Hermans et al.[27] Our experimental data in the temperature range of 236−600 K agree well with the theoretical results. The calculation results exhibit a negative temperature dependence over the present experimental temperature range.

From interpolating the rate constants between the high-temperature studies[15−17] and the present study, the reaction rate would have minimum value at temperatures between 600 and 1000 K and shows a positive dependence above that temperature. Such temperature dependence of the rate constants can be accomplished with a direct H-atom abstraction mechanism, which is a direct H atom transfer from the OH group of CH_2OH

to the O_2, leading to CH_2O and HO_2.[8,22] Although we have surveyed the direct H-atom abstraction pathway, it was not found on the doublet PES of the ground state. It is important to note that the direct H-atom abstraction pathway was not found by other theoretical studies as well.[8,26]

4. Conclusion

The kinetics of the reaction $CH_2OH + O_2 \rightarrow CH_2O + HO_2$ were investigated at 50 Torr of N_2 in the temperature range of 236−600 K using a single experimental setup. The reaction rate constants show slight negative temperature dependence. The μVTST/Master Equation calculations were performed on the basis of the doublet ground-state PES calculated at the G3//B3LYP/6-31G(d) level of theory. The theoretical results agreed well with our experimental measurements, suggesting an association/decomposition mechanism. The temperature dependences of the rate constants of the reaction of the hydroxymethyl radical with molecular oxygen determined in the present study have an impact in the estimate of the atmospheric formation of HO_2 and CH_2O. Further studies are desirable to elucidate the low-temperature methanol combustion mechanism above 600 K.

Acknowledgment. The authors gratefully acknowledge A. Tezaki (Toyama University) and K. Kohse-Höinghaus (Universität Bielefeld) for helpful discussions. K.T. thanks the General Sekiyu Research Promotion Foundation for financial support. A.S. thanks the German Science Foundation (Deutsche Forschungsgemeinschaft, DFG) and the German Chemical Society (Gesellschaft Deutscher Chemiker, GDCh) for financial support under the occasion of the "German year in Japan 2005/2006" (Deutschland in Japan 2005/2006-Jahr).

Supporting Information Available: Structures of reactants, intermediates, products, and transition states for the reaction of the hydroxymethyl radical with molecular oxygen and a table of total energies are available free of charge via the Internet at http://pubs.acs.org.

Note Added after ASAP Publication. This article was released ASAP on March 14, 2007. Figure captions 4 and 5 have been revised. The corrected version was posted on March 21, 2007.

References and Notes

(1) Atkinson, R. *Atmos. Environ. Part A*—Gen. Top. **1990**, *24*, 1.
(2) Kohse-Höinghaus, K.; Jeffries, J. B. *Applied Combustion Diagnostics*; Taylor and Francis: New York, 2002; see also references therein.
(3) Schocker, A.; Kohse-Höinghaus, K.; Brockhinke, A. *Appl. Opt.* **2005**, *44*, 6660.
(4) Fernandez-Ramos, A.; Miller, J. A.; Klippenstein, S. J.; Truhlar, D. G. *Chem. Rev.* **2006**, *106*, 4518.
(5) Atkinson, R.; Arey, J. *Acc. Chem. Res.* **1998**, *31*, 574.
(6) Carter, W. P. L.; Darnall, K. R.; Graham, R. A.; Winer, A. M.; Pitts, J. N., Jr. *J. Phys. Chem.* **1979**, *83*, 2305.
(7) Niki, H.; Maker, P. D.; Savage, C. M.; Breitenbach, L. P. *Chem. Phys. Lett.* **1981**, *80*, 499.
(8) Dibble, T. S. *Chem. Phys. Lett.* **2002**, *355*, 193.
(9) Grotheer, H. H.; Riekert, G.; Walter, D.; Just, T. *J. Phys. Chem.* **1988**, *92*, 4028.
(10) Westbrook, C. K.; Dryer, F. L. *Combust. Sci. Technol.* **1979**, *20*, 125.
(11) Held, T. J.; Dryer, F. L. *Int. J. Chem. Kinet.* **1998**, *30*, 805.
(12) Lindstedt, R. P.; Meyer, M. P. *Proc. Combust. Inst.* **2002**, *29*, 1395.
(13) Lu, C. W; Chou, S. L.; Lee, Y. P.; Xu, S.; Xu, Z. F.; Lin, M. C. *J. Chem. Phys.* **2005**, *122*, 244314.
(14) Radford, H. E. *Chem. Phys. Lett.* **1980**, *71*, 195.
(15) Tsuboi, T.; Hashimoto, K. *Combust. Flame* **1981**, *42*, 61.
(16) Vandooren, J.; van Tigglen, P. J. *Symp. (Int.) Combust.*, [*Proc.*], *18th* **1980**, 473.
(17) Olsson, J. O.; Olsson, I. B. M.; Ansersson, L. L. *J. Phys. Chem.* **1987**, *91*, 4160.
(18) Wang, W. C.; Suto, M.; Lee, L. C. *J. Chem. Phys.* **1984**, *81*, 3122.
(19) Grotheer, H. H.; Riekert, G.; Meier, U.; Just, T. *Ber. Bunsen-Ges. Phys. Chem.* **1985**, *89*, 187.
(20) Dóbe, S.; Temps, F.; Böhland, T.; Wagner, H. G. *Z. Naturforsch.* **1985**, *40*, 1289.
(21) Payne, W. A.; Brunning, J.; Mitchell, M. B.; Stief, L. J. *Int. J. Chem. Kinet.* **1988**, *20*, 63.
(22) Nesbitt, F. L.; Payne, W. A.; Stief, L. J. *J. Phys. Chem.* **1988**, *92*, 4030.
(23) Pagsberg, P.; Munk, J.; Anastasi, C.; Simpson, V. J. *J. Phys. Chem.* **1989**, *93*, 5162.
(24) Miyoshi, A.; Matsui, H.; Washida, N. *J. Phys. Chem.* **1990**, *94*, 3016.
(25) Hanoune, B.; Dusanter, S.; ElMaimouni, L.; Dovolder, P.; Lemoine, B. *Chem. Phys. Lett.* **2001**, *343*, 527.
(26) Olivella, S.; Bofill, J. M.; Solé, A. *Chem. Eur. J.* **2001**, *7*, 3377.
(27) Hermans, I.; Müller, J.-F.; Nguyen, T. L.; Jacobs, P. A.; Peeters, J. *J. Phys. Chem. A* **2005**, *109*, 4303.
(28) Ramírez-Ramírez, V. M.; Serrano-Andrés, L.; Nebot-Gil, I. *Theor. Chem. Acc.* **2006**, *116*, 637.
(29) Kanno, N.; Tonokura, K.; Tezaki, A.; Koshi, M. *J. Mol. Spectrosc.* **2005**, *229*, 193.
(30) Kanno, N.; Tonokura, K.; Tezaki, A.; Koshi, M. *J. Phys. Chem. A* **2005**, *109*, 3153.
(31) Kanno, N.; Tonokura, K.; Koshi, M. *J. Geophys. Res.* **2006**, *111*, D20312, doi:10.1029/2005JD006805.
(32) Suzaki, K.; Kanno, N.; Tonokura, K.; Koshi, M.; Tsuchiya, K.; Tezaki, A. *Chem. Phys. Lett.* **2006**, *425*, 179.
(33) Hunziker, H. E.; Wendt, H. R. *J. Chem. Phys.* **1974**, *60*, 4622.
(34) Fink, E. H.; Ramsay, D. A. *J. Mol. Spectrosc.* **1997**, *185*, 304.
(35) Avetisov, V. G.; Kauranen, P. *Appl. Opt.* **1996**, *35*, 4705.
(36) Kee, R. J.; Rupley, F. M.; Miller, J. A.; Coltrin, M. E.; Grcar, J. F.; Meeks, E.; Moffat, H. K.; Lutz, A. E.; Dixon-Lewis, G.; Smooke, M. D.; Warnatz, J.; Evans, G. H.; Larson, R. S.; Mitchell, R. E.; Petzold, L. R.; Reynolds, W. C.; Caracotsios, M.; Stewart, W. E.; Glarborg, P.; Wang, C.; Adigun, O.; Houf, W. G.; Chou, C. P.; Miller, S. F.; Ho, P.; Young, D. J. *CHEMKIN*, Release 4.0; Reaction Design, Inc.: San Diego, CA, 2004.
(37) Tyndall, G. S.; Orlando, J. J.; Kegley-Owen, C. S.; Wallington, T. J.; Hurley, M. D. *Int. J. Chem. Kinet.* **1999**, *31*, 776.
(38) Pagsberg, P.; Munk, J.; Sillesen, A.; Anastasi, C. *Chem. Phys. Lett.* **1988**, *146*, 375.
(39) Meier, U.; Grotheer, H. H.; Riekert, G.; Just, Th. *Ber. Bunsen-Ges. Phys. Chem.* **1985**, *89*, 325.
(40) Kircher, C. C.; Sander, S. P. *J. Phys. Chem.* **1984**, *88*, 2082.
(41) Tyndall, G. S.; Wallington, T. J.; Hurley, M. D.; Schneider, W. F. *J. Phys. Chem.* **1993**, *97*, 1576.
(42) Cox, R. A.; Burrows, J. P. *J. Phys. Chem.* **1979**, *83*, 2560.
(43) Stone, D.; Rowley, D. M. *Phys. Chem. Chem. Phys.* **2005**, *7*, 2156.
(44) Christensen, L. E.; Okumura, M.; Sander, S. P.; Salawitch, R. J.; Toon, G. C.; Sen, B.; Blavier, J.-F.; Jucks, K. W. *Geophys. Res. Lett.* **2002**, *29*, 1299.
(45) Desain, J. D.; Jusinski, L. E.; Ho, A. D.; Taatjes, C. A. *Chem. Phys. Lett.* **2001**, *347*, 79.
(46) Hsu, C. C.; Mebel. A. M.; Lin, M. C. *J. Chem. Phys.* **1996**, *105*, 2346.
(47) Gaboul, A. G.; Curtiss, L. A.; Redfern, P. C.; Rassolv, V. *J. Chem. Phys.* **1999**, *110*, 7650.
(48) Frisch, M. J.; Trucks, G. W.; Schlegel, H. B.; Scuseria, G. E.; Robb, M. A.; Cheeseman, J. R.; Montgomery, J. A., Jr.; Vreven, T.; Kudin, K. N.; Burant, J. C.; Millam, J. M.; Iyengar, S. S.; Tomasi, J.; Barone, V.; Mennucci, B.; Cossi, M.; Scalmani, G.; Rega, N.; Petersson, G. A.; Nakatsuji, H.; Hada, M.; Ehara, M.; Toyota, K.; Fukuda, R.; Hasegawa, J.; Ishida, M.; Nakajima, T.; Honda, Y.; Kitao, O.; Nakai, H.; Klene, M.; Li, X.; Knox, J. E.; Hratchian, H. P.; Cross, J. B.; Bakken, V.; Adamo, C.; Jaramillo, J.; Gomperts, R.; Stratmann, R. E.; Yazyev, O.; Austin, A. J.; Cammi, R.; Pomelli, C.; Ochterski, J. W.; Ayala, P. Y.; Morokuma, K.; Voth, G. A.; Salvador, P.; Dannenberg, J. J.; Zakrzewski, V. G.; Dapprich, S.; Daniels, A. D.; Strain, M. C.; Farkas, O.; Malick, D. K.; Rabuck, A. D.; Raghavachari, K.; Foresman, J. B.; Ortiz, J. V.; Cui, Q.; Baboul, A. G.; Clifford, S.; Cioslowski, J.; Stefanov, B. B.; Liu, G.; Liashenko, A.; Piskorz, P.; Komaromi, I.; Martin, R. L.; Fox, D. J.; Keith, T.; Al-Laham, M. A.; Peng, C. Y.; Nanayakkara, A.; Challacombe, M.; Gill, P. M. W.; Johnson, B.; Chen, W.; Wong, M. W.; Gonzalez, C.; Pople, J. A. *Gaussian 03*, Revision B.04; Gaussian, Inc.: Wallingford, CT, 2004.
(49) Anglada, J. M.; Domingo, V. M. *J. Phys. Chem. A* **2005**, *109*, 10786.
(50) Klippenstein, S. J.; Wagner, A. F.; Dunbar, R. C.; Wardlaw, D. M.; Robertson, S. H.; Miller, J. A. *VARIFLEX*, 1.13m ed.; 2002.